Available online at www.sciencedirect.com
SCIENCE DIRECT®
Biosensors and Bioelectronics 21 (2006) 1029–1036
BIOSENSORS & BIOELECTRONICS
www.elsevier.com/locate/bios

Counter-propagating optical trapping system for size and refractive index measurement of microparticles

Richard A. Flynn [a], Bing Shao [a,*], Mirianas Chachisvilis [a], Mihrimah Ozkan [b], Sadik C. Esener [a]

[a] *Department of Electrical and Computer Engineering, University of California, San Diego, La Jolla, CA 92093, USA*
[b] *Department of Electrical Engineering, University of California, Riverside, CA 92521, USA*

Received 14 December 2004; received in revised form 19 March 2005; accepted 23 March 2005
Available online 22 April 2005

Abstract

We propose and demonstrate a novel approach to measure the size and refractive index of microparticles based on two beam optical trapping, where forward scattered light is detected to give information about the particle. The counter-propagating optical trap measurement (COTM) system exploits the capability of optical traps to measure pico-Newton forces for microparticles' refractive index and size characterization. Different from the current best technique for microparticles' refractive index measurement, refractometry, a bulk technique requiring changing the fluid composition of the sample, our optical trap technique works with any transparent fluid and enables single particle analysis without the use of biological markers. A ray-optics model is used to explore the physical operation of the COTM system, predict system performance and aid system design. Experiments demonstrate the accuracy of refractive index measurement of $\Delta n = 0.013$ and size measurement of 3% of diameter with 2% standard deviation. Present performance is instrumentation limited, and a potential improvement by more than two orders of magnitude can be expected in the future. With further development in parallelism and miniaturization, the system offers advantages for cell manipulation and bioanalysis compatible with lab-on-a-chip systems.

Keywords: Optical trapping; Refractive index; Size; Scattering; Ray-optics; Mie theory

1. Introduction

As a non-invasive scientific tool capable of manipulating biological cells (Ashkin et al., 1987; Buican et al., 1987), bacteria (Ashkin and Dziedzic, 1987), organelles within cells (Ashkin et al., 1987; Ashkin and Dziedzic, 1989) and even viruses (Ashkin and Dziedzic, 1987), optical traps have not only been used to measure the smallest forces to date in biological realm (e.g. those of motor proteins) (Svoboda et al., 1994), but also been employed in the sorting of biological cells (Buican et al., 1987).

This work expands the capabilities of optical traps beyond manipulation and force measurement to refractive index and size characterization of the particle held in the trap, which enables analysis without using biological markers that may interfere with the biological function being studied. The aim is to create a useful tool for cell manipulation and bioanalysis compatible with the emerging lab-on-a-chip systems, in which a series of complex chemical or biological analysis steps can be carried out rapidly and effectively in a tiny, portable environment (Unger et al., 2000; Thorsen et al., 2002; Adams et al., 2002; Groisman et al., 2003).

In our counter-propagating optical trap measurement (COTM) system (Fig. 1), optical forces align a trapped particle to a particular position within the beam based on its refractive index and size, and the forward scattered light detected by the photodetector yields information about the particle. This aspect of the technique is similar with the forward scattered light measurement in flow cytometry (Shapiro, 2003), in which cells are driven past a laser beam by a fluid flow, and

* Corresponding author. Tel.: +1 858 822 4158; fax: +1 858 534 1225.
E-mail address: bshao@soliton.ucsd.edu (B. Shao).

0956-5663/$ – see front matter © 2005 Elsevier B.V. All rights reserved.
doi:10.1016/j.bios.2005.03.011

Report Documentation Page

Form Approved
OMB No. 0704-0188

1. REPORT DATE	2. REPORT TYPE	3. DATES COVERED
01 JUN 2005	**N/A**	**-**

4. TITLE AND SUBTITLE	5a. CONTRACT NUMBER
Counter-propagating optical trapping system for size and refractive index measurement of microparticles	5b. GRANT NUMBER
	5c. PROGRAM ELEMENT NUMBER
6. AUTHOR(S)	5d. PROJECT NUMBER
	5e. TASK NUMBER
	5f. WORK UNIT NUMBER
7. PERFORMING ORGANIZATION NAME(S) AND ADDRESS(ES) **Department of Electrical and Computer Engineering, University of California, San Diego, La Jolla, CA 92093, USA**	8. PERFORMING ORGANIZATION REPORT NUMBER
9. SPONSORING/MONITORING AGENCY NAME(S) AND ADDRESS(ES)	10. SPONSOR/MONITOR'S ACRONYM(S)
	11. SPONSOR/MONITOR'S REPORT NUMBER(S)

12. DISTRIBUTION/AVAILABILITY STATEMENT
Approved for public release, distribution unlimited

13. SUPPLEMENTARY NOTES
See also ADM001923.

14. ABSTRACT

15. SUBJECT TERMS

16. SECURITY CLASSIFICATION OF:			17. LIMITATION OF ABSTRACT	18. NUMBER OF PAGES	19a. NAME OF RESPONSIBLE PERSON
a. REPORT	b. ABSTRACT	c. THIS PAGE			
unclassified	**unclassified**	**unclassified**	**UU**	**8**	

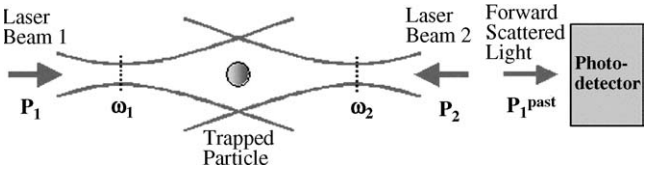

Fig. 1. Simple diagram of the COTM system. A photodetector captures the forward scattered light from the laser trap for measurement. P_1, power of laser beam 1; P_2, power of laser beam 2; ω_1, beam waist of laser beam 1; ω_2, beam waist of laser beam 2.

the forward scattered light, side scattered light and fluorescence are used to identify the cell or the presence of particular biomolecules within the cells. While in flow cytometry attempts are made to minimize the influence of refractive index on measurements (Shapiro, 2003) and focus merely on size, our approach focuses on both refractive index and size.

In this article, we present the theory of refractive index and size measurement using the COTM system together with numerical simulations of the axial force, the particle equilibrium position and the detected scattered light intensity signal (power) dependencies on the particle size and refractive index. Theoretical results are compared with measurements of refractive index and size of trapped dielectric microspheres using the COTM system. A remarkable agreement between the ray-optics simulations and the experimental results proves the ability of COTM system in accurately estimating the refractive index and size of a trapped particle from the detected scattered light power (intensity of forward scattered radiation). Noise analysis predicts that an improvement on measurement accuracy by more than two orders of magnitude is possible. The unique features of COTM system, such as the low requirements on numerical aperture, laser power, and working distance, endow it potential on future parallelism and miniaturization, which makes it a powerful and compatible research tool in lab-on-a-chip integrated cellular diagnosis.

2. Materials and methods

2.1. Theory and simulations

As the first stable optical trap demonstrated (Ashkin, 1970), two-beam optical trap holds a primary advantage over single-beam trap in that it can operate over a larger working distance (millimeter or more) since only weakly focused beams are required. In a counter-propagating two-beam trap, two focused laser beams propagate in opposite directions to create a 3D optical trap through a combination of axial and transverse forces. The operation basis of the counter-propagating optical trap measurement system presented here is to extract information about the trapped particle from the forward scattered light (Fig. 1).

According to the size of the particle to be trapped relative to the wavelength of the laser, physical models of optical traps break down into Rayleigh regime, intermediate regime and Mie regime. Based on the fact that biological cells size from 1 μm to 100 μm, this paper primarily deals with particles in between the Mie scattering regime and the intermediate regime.

In Mie regime, the wave nature of light such as interference and diffraction can be safely ignored (Saleh and Teich, 1991). Light is treated as traveling in straight lines, changing direction only at the interface between two materials, and optical forces (axial and transverse) arise from the momentum change of a photon upon reflection and refraction at a material boundary. The axial force due to reflection always pushes the particle forward, while the axial force due to refraction always pulls the particle toward the focus. When two weakly focused beams travel in opposite directions, a stable equilibrium position exists where the axial forces of the two beams cancel out.

In ray-optics modeling of the COTM system (Fig. 2A), the laser beam is broken down into a series of rays, each carries a portion of the power in a particular direction and is traced through the particle through infinite reflections and refractions at the particle/medium interface. Adding up the

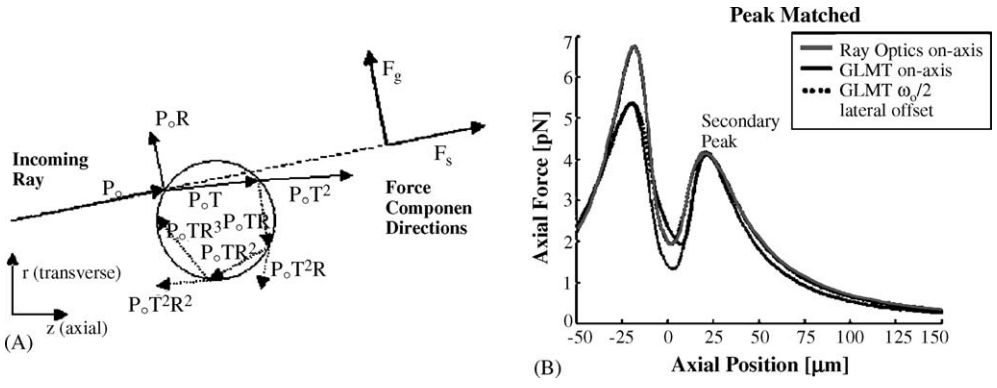

Fig. 2. Ray-optics model and its validity. (A) Force components of a single ray on a microsphere. Gradient, F_g, and scatter, F_s, component directions are relative to angle of incoming ray. P_o, power of an incident ray; R, Fresnel coefficient of reflection; T, Fresnel coefficient of transmission. (B) GLMT to ray-optics comparison. Fitting the peaks shows good match to the right of the secondary peak.

forces from each ray yields the total optical force executed on the particle.

To testify the validity of applying ray-optics in our system, where the particle size is not always much larger than the wavelength, the ray-optics model is compared to the intermediate regime model, Generalized Lorenz–Mie Theory (GLMT) (Ren et al., 1996). Since the COTM system operates only to the right of the secondary force peak, and the equilibrium position of the particle is determined by the shape instead of the magnitude of axial force, all comparison focus on the shape differences between GLMT and ray-optics in this region. Accordingly, the two models' estimations of the axial force on a 5 μm diameter particle (larger particles should yield better match due to the increased validity of ray-optics model) in Fig. 2B prove the ray-optics model as a reasonable approximation for the COTM system.

GLMT simulations in Fig. 2B also show that small lateral offset of the particle does not alter the axial force curve in the interested region, which alleviates the concern that small lateral offset caused by gravity might affect the accuracy in assuming "on-axis trapping" for the ray-optics model.

In the COTM system (Fig. 1), a photodetector detects the forward scattered light power from the two-beam trap to provide information about the trapped particle. A ray-based simulation is used to describe forces on the particle, find its equilibrium position, and establish the dependency of the detected power on the refractive index and size of the particle and the power of beam 2.

According to the ray-optics model (Fig. 2A), the scattering and gradient force exerted by a single ray on a sphere (Saleh and Teich, 1991)

$$F_s = \frac{n_1 P}{c}\left\{1 + R\cos 2\theta_i - \frac{T^2\,[\cos(2\theta_i - 2\theta_r) + R\,\cos 2\theta_i]}{1 + R^2 + 2R\,\cos 2\theta_r}\right\} \quad (1)$$

$$F_g = \frac{n_1 P}{c}\left\{R\,\sin 2\theta_i - \frac{T^2\,[\sin(2\theta_i - 2\theta_r) + R\,\sin 2\theta_i]}{1 + R^2 + 2R\,\cos 2\theta_r}\right\} \quad (2)$$

results from infinite number of internal reflections and refractions (Ashkin, 1992). Variables here are n_1, refractive index of surrounding medium, θ_i, angle of incidence, θ_r, angle of refractions, c, the velocity of light, R and T are the Fresnel coefficients for reflection and transmission, respectively.

The axial force is found by adding the axial components of the gradient and scattering forces and scales linearly with the beam power

$$F_s^{axial} = F_s\,\cos\phi \quad (3)$$

$$F_g^{axial} = -F_g\,\sin\phi \quad (4)$$

$$F_{axial} = F_s^{axial} + F_g^{axial} \quad (5)$$

where ϕ is the angle between the ray and the axis (direction of the laser beam).

With parameters used in the experiment, Gaussian beam divergence half angle in air, $\phi_{div} = 10.95^\circ$, total beam power, $P_{beam} = 9.6$ mW, microsphere diameter, $D = 5$ μm, and microsphere refractive index (polystyrene), $n_2 = 1.59$, the axial force exerted by a Gaussian beam is shown as the gray curve in Fig. 2B.

To estimate the detected optical power, any ray leaving the sphere and passing through the aperture (microscope objective in the COTM system) is assumed to reach the detector. Since the majority of power in the forward direction is $P_o T^2$ (Fig. 2A), only this component is detected. The remainder is approximated as isotropically scattered in all directions, with a negligible amount scattered in the forward direction through the aperture.

The detected power is influenced by two factors: (1) the equilibrium position of the microsphere determined by the dependence of axial force on axial position and (2) the dependence of equilibrium position on the power ratio between two beams. These are combined to plot detected power versus power ratio, the curve to be measured by the COTM system.

During the operation, a stable equilibrium position is created between the two beam foci. Small displacement to either side results in a force restoring the sphere back. Controlled by the power ratio ($R = P_2/P_1$) of the beam powers (Fig. 3A and B), the equilibrium position is located at the midpoint between the two beam foci at power ratio of 1, moving towards the focus of beam 2 as R is reduced. COTM system utilizes power ratios that keep the equilibrium position between the secondary peaks so that an optimized resolution can be obtained (Flynn, 2004).

The sphere acts as both a scattered reflecting light at various angles, and a lens focusing transmitted light. Detected power is normalized to the value obtained without the sphere, since in this case the output aperture still clips some of the beam, the normalized power of one represents less than the full input power. The detected power curve consists of a single peak surrounded by two valleys roughly corresponding to the two peaks in axial force (Fig. 2B). When the sphere is at the focus, the rays strike normal to the surface, low reflectivity and little change in ray orientation makes the detected power close to one. Moving past the focus, the bead focuses more light through the aperture and the normalized detected power exceeds one. Right after the peak position, increased scattering dominates over the focusing effect and the detected power drops to a minimum. At large distances from the focus, the detected power increases monotonically and asymptotically approaches one because more beam power misses the sphere and is fully collected (Fig. 3C).

An almost linear relationship between detected power and the ratio of powers of two laser beams (Fig. 3D) is obtained by combining the detected power versus position relationship (Fig. 3C) with the equilibrium position versus power ratio relationship (Fig. 3B). The variation of slope and level with the

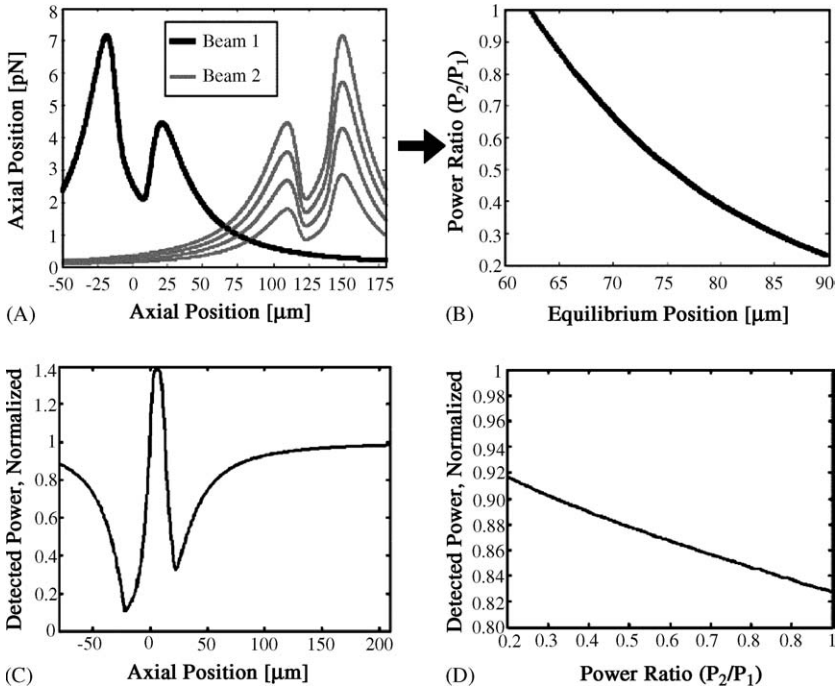

Fig. 3. Ray-optics simulations. (A) Axial position vs. axial force. The shift of the axial position of the stable equilibrium with changing of power ratio P_2/P_1 is illustrated clearly in the plot. (B) Equilibrium position of the microsphere as power ratio is reduced. (C) Normalized detected power vs. axial position. (D) Normalized detected power vs. power ratio of two laser beams.

refractive index and size of the particle forms the operation basis for the COTM system.

Simulations on the detected power versus axial position curves (Fig. 4A) reveals virtually unchanged positions of peaks and valleys and a non-linear scaling of the detected power as the refractive index changes. The dependence of scattered light power on the power ratio between two laser beams is shown in Fig. 4C. The large differences between curves for indices close to that of water ($n = 1.33$) suggests high resolution in detection of biological particles whose

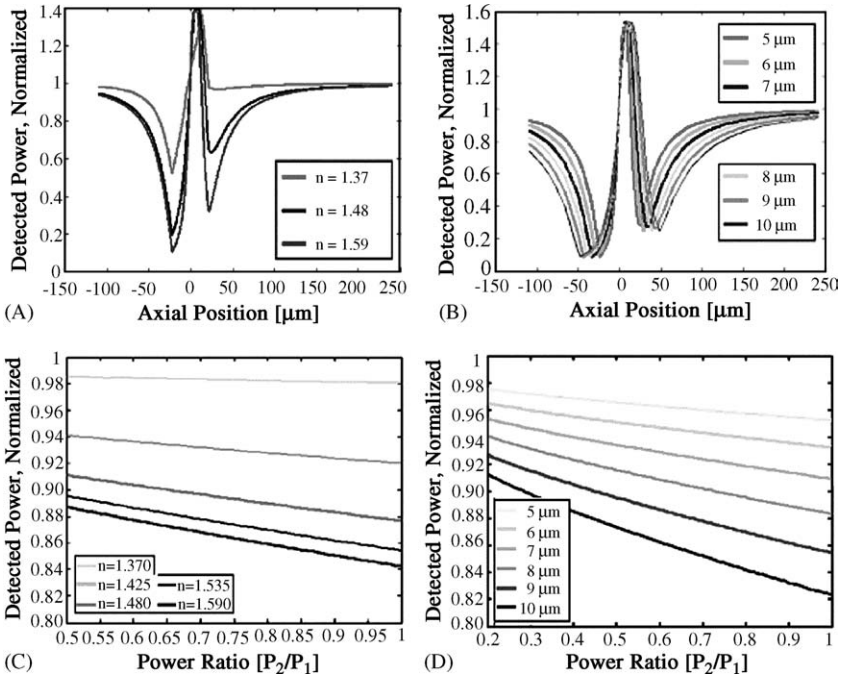

Fig. 4. Ray-optics simulations. Variation of normalized detected power vs. axial position with (A) refractive index and (B) size of microspheres. Variation of normalized detected power vs. power ratio with (C) refractive index and (D) size of microspheres.

indices are close to that of water. Refractive index differences on the order of 0.01 should be easily detectable, especially in the neighborhood of 1.37–1.48 indices.

Changes in particle size stretch the detected power versus position curve linearly along the axial direction without changing the height of the peaks and valleys (Fig. 4B). The level and slope of detected power versus power ratio varies nearly linearly with size (Fig. 4D). Considering a typical A/D converter with a resolution of 0.0001, size difference smaller than 1 μm (which corresponds to a difference in normalized detected power smaller than 0.02) should be measurable in the system.

2.2. Experimental

As an important parameter in designing system, beam focus separation is determined based on the trade off between resolution and maximum measurable size. The locations of secondary axial force peaks of the two beams get closer as the particle size increases (Flynn, 2004), therefore the closer the beam foci locate, the smaller the upper limit for trappable size is. On the other hand, a smaller beam focus separation puts the equilibrium position closer to the secondary axial force peak, where the detection resolution is higher (Fig. 4A and B). Buoyancy forces due to different density of measured particles also affect the decision on the beam focus separation (Flynn, 2004). In this work, beam focus separation of 264 μm is chosen for the size setup to accommodate spheres that are 10 μm or larger for size measurement, while for the refractive index setup, a beam focus separation of 131 μm is used to obtain enough transverse force to overcome the large negative buoyancy possessed by high density particles, like borosilicate glass and silica (near 2.00 g/cm^3 and 2.50 g/cm^3, respectively).

A practical implementation of the COTM system includes: (1) two weakly focused counter-propagating beams with adjustable relative power, (2) detection of the scattered light from one of the beams, and (3) a side-imaging system.

As shown in Fig. 5, the laser beam from a diode laser (λ = 850 nm, SDL Inc., San Jose, CA) is reshaped with beam shaping optics (Flynn, 2004) to form a Gaussian beam, which is then split by a beamsplitter and focused through two microscope objectives MO1 and MO2 (DIN 20×, NA = 0.4, Edmund Optics Inc., Barrington, NJ) from opposite directions. The relative beam power is controlled by a pair of crossed polarizers (Part number 03 FPI 001, λ = 780–1250 nm, Melles Griot, Calsbad, CA) in the path of beam 2. The optical trap is formed in a square capillary tube (Part number 8100–050, l = 50 mm, VitroCom Inc., Mountain Lakes, NJ) with 1 mm inner diameter and 200 μm sidewall thickness, which holds the solution of particles to be analyzed. MO2 focuses beam 2, and collects the forward scattered light from beam 1 (light gray path in Fig. 5). The scattered light is then directed to a photodetector (Model number 1830-C, Newport Corp., Irvine, CA) by a pellicle beamsplitter (Part number 03BPL001, Melles Griot). The side-imaging part consists

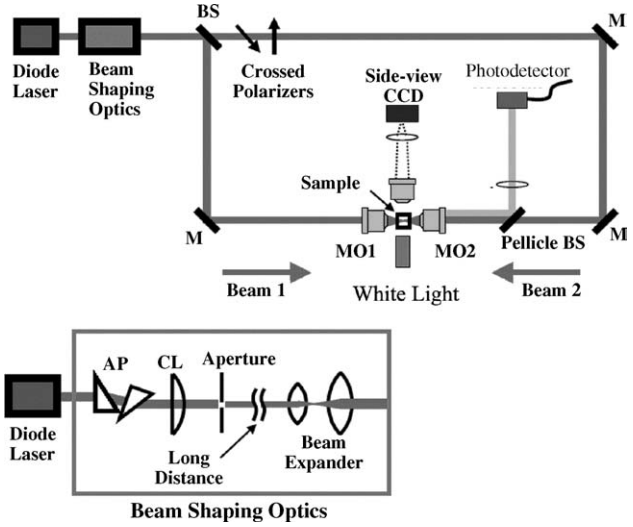

Fig. 5. Schematic of COTM system. Inset at bottom gives details of the beam shaping optics. BS, beam splitter; M, mirror; MO, microscope objective; AP, anamorphic prism; CL, cylindrical lens.

of a white light source (Fiber-Lite, Model 3100, Dolan-Jenner Industries Inc., Lawrence, MA), a microscope objective MO3 (Plan-Fluor, 10×, NA = 0.30, WD = 0.16, Nikon, Japan), and a CCD camera (Model number TM-200NIR, Pulnix, Sunnyvale, CA). By viewing the particle trajectory along the optical axis, axial force curves of both beams can be measured and their axial spacing indicates the beam focus separation.

For refractive index measurements, microspheres of silica (Cat. number SS05N, Bangs Laboratories Inc., Fishers, IN), borosilicate glass (Cat. number 9005, Duke Scientific Corp., Palo Alto, CA) and polystyrene (Cat. number 4205A, Duke Scientific Corp.), all with 5 μm nominal diameter are used. The refractive index of each material at 589 nm wavelength is 1.37 for silica, 1.56 for borosilicate glass and 1.59 for polystyrene. For size measurements, polystyrene particles of diameter 5–10 μm with 1 μm increments (Cat. number 4205A-4210A, Duke Scientific Corp.) are used.

Microspheres to be measured are suspended in the solution (D.I. water) at appropriate concentration and injected into the cuvette. A microsphere is then found and trapped by moving the cuvette with a 3D stage (Model number 460P-XYZ, Newport Corp.).

Measurement consists of reading the forward scattered light for a series of power ratios P_2/P_1. By rotating the crossed polarizers, power ratio can be adjusted from 2% to 100%. Data from the photodetector is recorded by a PC using Labview (National Instruments Inc.).

3. Results

Fig. 6 shows the results of index and size measurement. Curves are based on five samples of each microsphere type

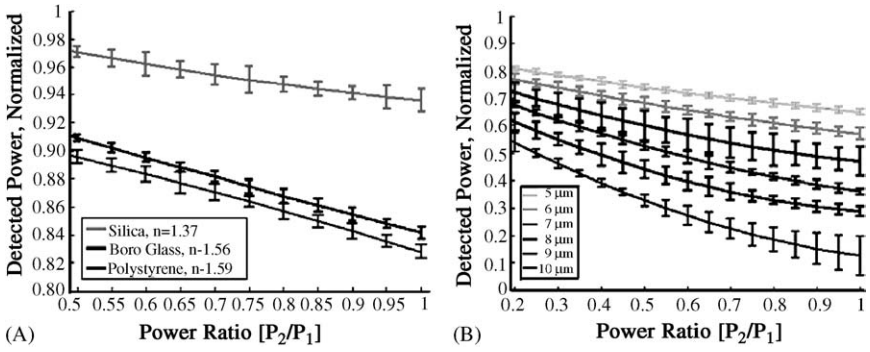

Fig. 6. Experimental results for (A) refractive index and (B) size measurement.

normalized by power reading without microsphere. Each curve is a second order polynomial fit to the mean value of the five readings with error bars representing standard deviations at corresponding power ratios. From Fig. 6A, the average standard deviation of the normalized detected power in refractive index calibration measurement is 0.49%. While in Fig. 6B, the average standard deviation of the normalized detected power is 2% for size calibration measurement.

These measurements reflect the ability of the COTM system to differentiate particles based on their refractive index and size, and form the basis of estimating the index and size of a trapped particle. The resolution between the curves is sufficient to predict refractive index differentiation better than $\Delta n = 0.03$ and size differentiation better than 1 μm. The ultimate accuracy depends on the noise in the signal and the stability of the system.

The index and size estimation is based on the observation that the detected power versus power ratio dependencies exhibits continuous change. The refractive index, n, or size, d (diameter), at any given power ratio, R, and detected power, P, can be described by

$$n(P, R) = f_1(P, R) \tag{6}$$

$$d(P, R) = f_2(P, R) \tag{7}$$

Due to the continuous variation of power with index or size of the particle, a second order polynomial can be used as an approximation to functions f_1 and f_2,

$$n(P, R) = a_1(R)P^2 + b_1(R)P + c_1(R) \tag{8}$$

$$d(P, R) = a_2(R)P^2 + b_2(R)P + c_2(R) \tag{9}$$

where a_1, b_1, c_1 and a_2, b_2, c_2 are weighting coefficients differing with power ratio R.

Use index estimation as example for illustration, to calibrate, one measurement is performed on each known microsphere type: silica, borosilicate glass, and polystyrene microspheres. This generates three calibration datasets $P_1(n_1, R)$, $P_2(n_2, R)$ and $P_3(n_3, R)$. For each power ratio, R_i, a second order polynomial fit is performed with inputs n_1, $P_1(R_i)$; n_2, $P_2(R_i)$; n_3, $P_3(R_i)$, and a set of weighting coefficients $a_1^i(R_i)$, $b_1^i(R_i)$, $c_1^i(R_i)$ is extracted. Upon the completion of the calibration process, a full set of weighting coefficients, $a_1^i(R_i)$, $b_1^i(R_i)$, $c_1^i(R_i)$ is applied to the second order polynomial describing refractive index (Eq. (8)). When an unknown microsphere is measured, an estimate of the refractive index

$$n(P_i, R_i) = a_1^i(R_i)P^2 + b_1^i(R_i)P + c_1^i(R_i) \tag{10}$$

is obtained for each pair of P_i, R_i values by applying the second order polynomial model. The final refractive index estimate

$$n_{\text{est}} = \sum_{i}^{I} \frac{n(P_i, R_i)}{I} \tag{11}$$

is the mean value of the index estimates from each P_i, R_i value (I is the total number of data sets), which represents a best fit between the calibration data and the measurement data of the unknown microsphere.

Fig. 7A displays the experimentally determined index values. Measurement is then taken for 10 microspheres in a random order. A horizontal line represents the nominal refractive index of each microsphere material, gray-scale-coded with circles representing the index estimates. Estimates for each material cluster near the appropriate refractive index, with a variation as expected from the error bars in detected power versus power ratio measurements (Fig. 6A). Table 1 shows the nominal value along with the mean and standard deviation of the estimates. The results are accurate within the second decimal of the nominal value. The error of estimate is 0.006–0.013 with a standard deviation from 0.005 to 0.012. The accuracy of index estimation can be improved by using a larger number of materials for calibration, since more data points would reduce the error in the second order polynomial fit.

For size estimation, an image-processing technique is used to setup the standard of comparison so that errors due to size variations in the microsphere populations are mitigated.

Table 1
Refractive index estimate data

Material	Silica	Borosilicate Glass	Polystyrene
Nominal n	1.37	1.56	1.59
Mean estimate n	1.363	1.573	1.584
Standard deviation	0.0124	0.0051	0.0053

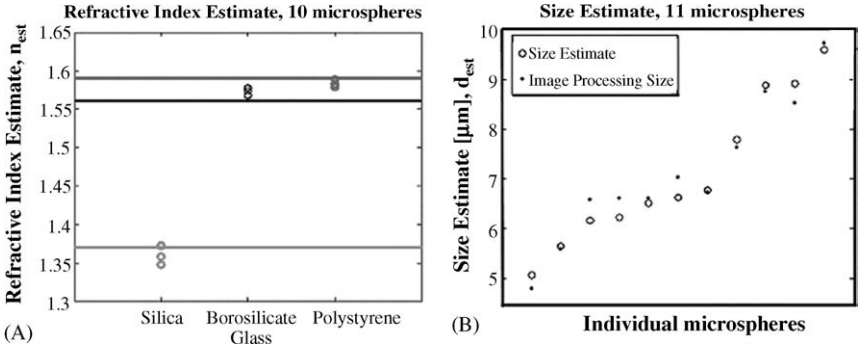

Fig. 7. Results of estimation experiments. (A) Calibrated refractive index estimate. Four silica, 3 borosilicate glass and 3 polystyrene particles are measured. Horizontal lines show the nominal refractive index of each material. (B) Calibrated size estimate. Size estimates are within less than 500 nm of the image processing estimates.

Size measurement is made with Metamorph (Universal Imaging Inc.) from still images of microspheres taken with the side-imaging system. According to the magnification of the size-imaging path, a pixel on the CCD corresponds to about 0.6 μm; therefore, a one-pixel error is 6–12% of microsphere size, depending on the diameter.

As shown in Fig. 7B, the COTM results cluster close to the image processing measurements for all sizes. Defining error_d as the absolute value of the difference between the size estimate d_1, and image processing size measurement d_2, divided by their average, for each data point

$$\text{error}_d = 2\left|\frac{d_1 - d_2}{d_1 + d_2}\right| \tag{12}$$

The average error over all 11 microspheres is 3.3%, with a standard deviation of 2.3%, which is within a single pixel error of the image processing size measurement, 6–12%. The accuracy and deviation of estimation can be improved by increasing the ratio between the number of measured samples and the number of particle types, which is relatively small for the case in Fig. 7B (11 over 5). Also, the image processing sizes are not error free because the threshold levels used for particle-background isolation have to be determined subjectively by the operator.

4. Discussion

The potential accuracy of the COTM system is limited by the noise of a direct laser to detector link. When the diode laser is pointed directly at the photodetector, the variation in detected power has a normalized standard deviation of about 0.0138% over 1 day. If the rest of the system adds no additional noise or variation over time, an overall uncertainty of 0.0138% standard deviation is possible, which corresponds to an error of ±0.0276% for a 95% confidence interval. From the simulation results on detected power versus power ratio for various refractive indices and sizes, at index close to a biological cell, i.e. $n = 1.37$, a 1% detected power change corresponds to $\Delta n = 0.0092$. For size measurement in the 5–10 μm range, a 1% detected power change corresponds to $\Delta d = 0.36$ μm. Accordingly, refractive index changes as small as ±0.00025 and size changes as small as ±10 nm could be detected if the detected power stability is within ±0.0276% (Flynn, 2004). Such sensitivities are comparable to that of a refractometer (Misco, 2004) for refractive index measurement and image processing techniques for size measurement. Even better, COTM holds the unique advantage over conventional technologies with its capability of marker-free single microparticle characterization in whatever transparent buffer is required by a living cell, eliminating the necessity of changing the fluid composition of the sample and monitoring particles via a microscope in refractometry, and of tagging a target with toxic fluorescence dyes in flow cytometry. All these features make our system extremely attractive for biomedical analysis. Since the COTM system measures index and size of particles in its original buffer media, and without a biomarker, it is more friendly to living cell analysis when compared to traditional technologies such as refractometry and flow cytometry. To be more specific, when measuring the index of a cell with the COTM system, one can keep the cell in its original buffer medium instead of having to add sucrose to the solution to make its refractive index match that of the cell (which is the case in refractometry and will most probably kill or alter the functioning of the subject cell). Also, when a particular drug is tested on a cell, the refractive index or size change induced by the drug effect will be indicated by a change in the detected forward scattered power. To accurately measure a drug's effect, it is absolutely necessary to maintain of cell's living ambient and its biological function, which would be changed dramatically by adding biomarkers like fluorescence dye or index matching compositions such as sucrose.

According to our simulation and experimental results (Figs. 4A and C and 6A), the COTM system is particularly sensitive to refractive index changes in the index range typical for biological cells. Researchers at Genoptix (Wang et al., 2003) have shown that cancerous and non-cancerous cells have different refractive indices, and even the level of drug response of a cell can be distinguished through refractive index. Clearly, measurements to differentiate biological cells and characterize drug response offer promising directions for future research using the COTM system.

5. Conclusions

The novel idea of using forward scattered light to measure the refractive index and size of the particle trapped in the COTM system has been suggested and proved both theoretically and experimentally. The accuracy of applying the ray-optics model to the analysis of our system was justified by comparison with the rigorous GLMT model.

The sensitivity of our system is 0.006–0.013 with 0.005–0.012 standard deviation for refractive index measurements and 3.3% of diameter with 2.3% standard deviation for size measurements. Noise analysis of the system predicts a potential improvement of refractive index estimation accuracy to within $\Delta n = \pm 0.00025$ for biological cells and size estimation accuracy to within $\Delta d = \pm 10$ nm. These accuracies compare favorably with current bulk techniques of index measurement with the further advantage of operating on a single microparticle in a variety of transparent fluids, which is an essential feature demand by live-cell analysis.

The COTM system is compatible with microfluidic systems where cells get analyzed, sorted and collected on one single chip. This kind of optical measurement allows probing of cells with no markers, so cells can be diagnosed without being altered. We believe that miniaturized version of the COTM system could offer a valuable tool for lab-on-a-chip bioanalysis in the future. Because two-beam optical trapping has low requirement on numerical aperture and working distance of focusing lens, it is promising to designing a COTM system implemented with VCSEL arrays and micro-optics for both miniaturization and high throughput.

Acknowledgement

The Defense Advances Research Project Administration (DARPA) via the CHIPS Optocenter and the University of California, San Diego, supported this work.

References

Adams, M., Derose, G., Quake, S.R., Scherer, A., 2002. Fundamental approach for optoelectronic and microfluidic integration for miniaturizing spectroscopic devices. Proc. SPIE 4647, 1–6.

Ashkin, A., 1970. Acceleration and trapping of particles by radiation pressure. Phys. Rev. Lett. 24, 156–159.

Ashkin, A., 1992. Forces of a single-beam gradient laser trap on a dielectric sphere in the ray-optics regime. Biophys. J. 61, 569–582.

Ashkin, A., Dziedzic, J.M., 1987. Optical trapping and manipulation of viruses and bacteria. Science 235, 1517–1520.

Ashkin, A., Dziedzic, J.M., 1989. Internal cell manipulation using infrared laser traps. In: Proceedings of the National Academy of Sciences, vol. 86, pp. 7914–7918.

Ashkin, A., Dziedzic, J.M., Yamane, T., 1987. Optical trapping and manipulation of single cells using infrared laser beams. Nature 330, 769–771.

Buican, T.N., Smyth, M.J., Crissman, H.A., Salzman, G.C., Stewart, C.C., Martin, J.C., 1987. Automated single-cell manipulation and sorting by light trapping. Appl. Opt. 26, 5311–5316.

Flynn, R.A., 2004. Measurement of refractive index and size of microparticles by optical traps generated by vertical cavity surface emitting lasers. Ph.D. Thesis, University of California, San Diego.

Groisman, A., Enzelberger, M., Quake, S.R., 2003. Microfluidic memory and control devices. Science 300, 955–958.

Misco, Home page: www.misco.com, April 2004.

Ren, K.F., Grehan, G., Gouesbet, G., 1996. Prediction of reverse radiation pressure by generalized Lorenz–Mie theory. Appl. Opt. 35, 2702–2710.

Saleh, B.E.A., Teich, M.C., 1991. Fundamentals of Photonics. Wiley, New York.

Shapiro, H.M., 2003. Practical Flow Cytometry, fourth ed. Wiley-Liss, Hoboken, NJ.

Svoboda, K., Mitra, P.P., Block, S.M., 1994. Fluctuation analysis of motor protein movement and single enzyme-kinetics. In: Proceedings of the National Academy of Sciences, vol. 91, pp. 11782–11786.

Thorsen, T., Maerki, S.J., Quake, S.R., 2002. Microfluidic large-scale integration. Science 298, 580–584.

Unger, M.A., Chou, H., Thorsen, T., Scherer, A., Quake, S.R., 2000. Monolithic microfabricated valves and pumps by multilayer soft lithography. Science 288, 113–116.

Wang, M.M., Schnabel, C.A., Chachisvilis, M., Yang, R., Paliotti, M.J., Simons, L.A., McMullin, L., Hagen, N., Lykstad, K., Tu, E., Pestana, L.M., Sur, S., Zhang, H., Butler, W.F., Kariv, I., Marchand, P.J., 2003. Optical forces for noninvasive cellular analysis. Appl. Opt. 42, 5765–5773.